Peer-reviewed version available at Symmetry 2020, 12, 768; doi:10.3390/sym12050768

Application of Fractional Derivative Without Singular and Local Kernel to Enhanced Heat Transfer in CNTs Nanofluid Over an Inclined Plate

Muhammad Saqib[1], Abdul Rahman Mohd Kasim[2], Nurul Farahain Mohammad[3], Dennis Ling Chuan Ching[4], and Sharidan Shafie[1,*]

[1]*Department of Mathematical Sciences, Faculty of Science, Universiti Teknologi Malaysia, Skudai 81310 UTM Johor Bahru, Malaysia*

[2]*Centre of mathematical sciences, Universiti Malaysia Pahang,26300, Lebuhara Tun Razak' Gambang, Kuantan Pahang*

[3]*Department of computational and theoretical sciences' International Islamic Universiti Malaysia; 25200, Kuantang Pahang*

[4]*Fundamental and applied sciences department; Universti Teknologi PETRONAS, Perak 32610, Malaysia*

***Corresponding author:** Sharidan@utm.my*

Abstract. Nanofluids are a novel class of heat transfer fluid that plays a vital role in industries. In mathematical investigations, these fluids are modeled in terms of traditional integer-order partial differential equations (PDEs). It is recognized that traditional PDEs cannot decode the complex behavior of physical flow parameters and memory effects. Therefore, this article intends to study the mixed convection heat transfer in nanofluid over an inclined vertical plate via fractional derivatives approach. The problem in hand is modeled in connection with Atangana-Baleanu fractional derivatives without singular and local kernel having strong memory. The human blood is considered as base fluid dispersing carbon nanotube (CNTs) (single-wall carbon nanotubes (SWCNTs) and multi-wall carbon nanotubes(MWCNTs)) into it to form blood-CNTs nanofluid. The nanofluids are considered to flow in a saturated porous medium under the influence of an applied magnetic field. The exact analytical expressions for velocity and temperature profiles are acquired using the Laplace transform technique and plotted in various graphs. The empirical results indicate that the memory effect decreases with increasing fractional parameters in the case of both temperature and velocity profiles. Moreover, the temperature profile is higher for blood-SWCNTs by reason of higher thermal conductivity whereas, this trend is opposite in case of velocity profile due densities difference.

Keywords: *Enhance heat transfer; Nanofluids; CNTs; Fractional derivatives; Laplace transform*

1. Introduction

In mixed convection regimes, enhanced heat transfer is significant for energy savings operations in industries. The primary constraint of traditional heat transfer fluid is poor thermal

conductivity which influences the mixed convection process [1]. Overcoming the flaws of traditional heat transfer fluids, nanofluid is a novel category of fluids which play its role in altering thermal feature of traditions fluids as illustration water, oils, alcohol, and ethylene glycol [2,3]. The surveys have indicated that the usages of nanofluids outcome the progress of execution of heat coolant of electronics and heat exchanger [4-6]. The procedure of heat transfer alteration can take into account by utilization of porous medium, employment of magnetic field and amending the thermophysical properties through nanomaterials (for instance, oxide, silica, carbid ,metals, non-metals, graphene and carbon nano tubes (CNTs) nanometer sized particles) [7]. The contemporary utilization of nanofluids and forces for examples magnetic field and porous medium to strengthen the thermal properties of heat exchanger have been debated in the literature .

Alzahrani et al. [8] studied single-wall carbon nanotubes (SWCNTs) and multi-wall carbon nanotubes (MWCNT) in water as a base fluid within parallel horizontal rotating plates. The inertia characteristics, microstructure, heat absorption/consumption, and thermal radiation are assumed. The problem models in the form of partial differential equations (PDEs), then transformed into ordinary differential equations (ODEs) and handle with Homotopy Analysis Method (HAM). It was indicated that the velocity profile decreases with increasing volume concentration and whereas the temperature profiles behave oppositely. Gul et al. [9] examined the flow water-based SWCNTs and MWCNTs nanofluids with variable temperature over a needle. The principal equations of the problem were modeled in the form of Caputo-Fractional derivatives and solved for numerical solutions. They pointed out that the impact of numerous physical flow parameters is restricted in the case of traditional derivatives. However, in the case of Caputo fractional derivatives, the influence of these parameters diverse at contrary intervals. Hassanan et al. [10] investigated the flow of oil-CNTs (SWCNT and MWCNTs) nanofluid over a stretching sheeting along with magnetohydrodynamic (MHD) and radiations effects. It was noticed that energy enhancement in oil-SWCNTs was higher than oil-MWCNTs due to high thermal conductivity, but the trend was opposite for velocity profile due to the difference in densities. Jabbari et al. [11] analyzed the viscosity of water-based SWCNTs by means of equilibrium molecular dynamics simulation. The viscosity variation was made for 0.125-0.734% SWCNTs nanofluids at temperature 25-65C^0. They reported that the viscosity of nanofluid increases with a high-volume fraction of SWCNTs at low temperatures. Kumam et al. [12]

carried out entropy generation and the second law of, thermodynamics application for kerosene oil-SWCNTs and kerosene oil-MWCNTs flow in a rotating microchannel. They considered source/sink, radiation and magnetic field effect. Their results shown that the velocity function reduced with Reynold number and entropy generation increases with Reynold, and Brinkman numbers. The interesting applications of CNTs nanofluid can be found in the review papers [13-15] and the reference therein.

The CNTs feature considerable mechanical and electrical thermal conduct forming a hexagonal cylinder network of carbon atoms 100 nm in length and 1nm in the bore. The major application of CNTs listed additives in polymers, nanolithography, hydrogen storage, supercapacitor, lithium-battery anodes and drug delivery [16]. Murshed [17] mention in the review paper that CNTs nanofluids have six-time higher thermal conductivity compared to other materials at ambient temperature. The CNTs nanofluids sufficiently investigated in the literature (see for example Xie et al. [18], Sarafraz et al. [19], Selimefendigil, and Öztop [20], Ghazali et al. [21] and Abdeen et al. [22]) but without memory and heredity effect. This is since, in mathematical studies, the traditional models with integer-order PDEs are utilized. These models can improve by using the applications of fractional derivatives. It is approved in the previous literature that fractional derivatives model can explain efficiently the real-world problem comprising electrical networks, diffusive transport, probability, electromagnetic theory, rheology, viscoelastic materials and fluid flow [23-29]. In the literature, several approaches for fractional derivatives are presented but the most common are the Riemann-Liouville [30], the Caputo [31,32], the Caputo-Fabrizio [33] and Atangana-Baleanu [34] fractional derivatives approaches. Among them, the most recent is Atangana-Baleanu fractional derivative without local and singular kernel having strong heredity and memory effect.

For the problem in hand, the Atangana-Baleanu fractional derivative approach is chosen due to non-locality, non-singularity and strong heredity and memory effect. A fractional Casson fluid model is developed for human blood-CNTs nanofluid associated with physical initial and boundary conditions. The model is solved for exact solutions via the Laplace transform technique. The analytical results are displayed in graphs with physical arguments.

Preprints (www.preprints.org) | NOT PEER-REVIEWED | Posted: 7 April 2020 doi:10.20944/preprints202004.0088.v1

Peer-reviewed version available at Symmetry 2020, 12, 768; doi:10.3390/sym12050768

2. Description of the Proposed Model

Consider the unsteady mixed convection flow of blood bases CNTs nanofluid over an inclined vertical plate with isothermal temperature T_∞ (room temperature/ ambient temperature). The half-space of the plate is filled with packed with human blood with SWCNTs and MWCNT with a saturated porous medium. The nanofluid is assumed to be electrically conducting. Hence, a magnetic field $\sigma_{nf} B_0^2 \sin(\gamma)$ of strength B_0 and direction γ is applied to the flow direction. The applied magnetic field due to polarization is ignored due to the very small Reynolds number. At the beginning at $t \le 0$, the system is in the rest position. But since the short interval t^+, the inclined plate oscillates with $U_0 H(t)\cos(\omega t)$ and the ambient temperature of the plate T_∞ rises to T_W. By the virtue of rising in temperature and oscillation of the plate, the mixed convection uncoils and the nanofluid starts motion in the upper direction as exhibited in Figure 1.

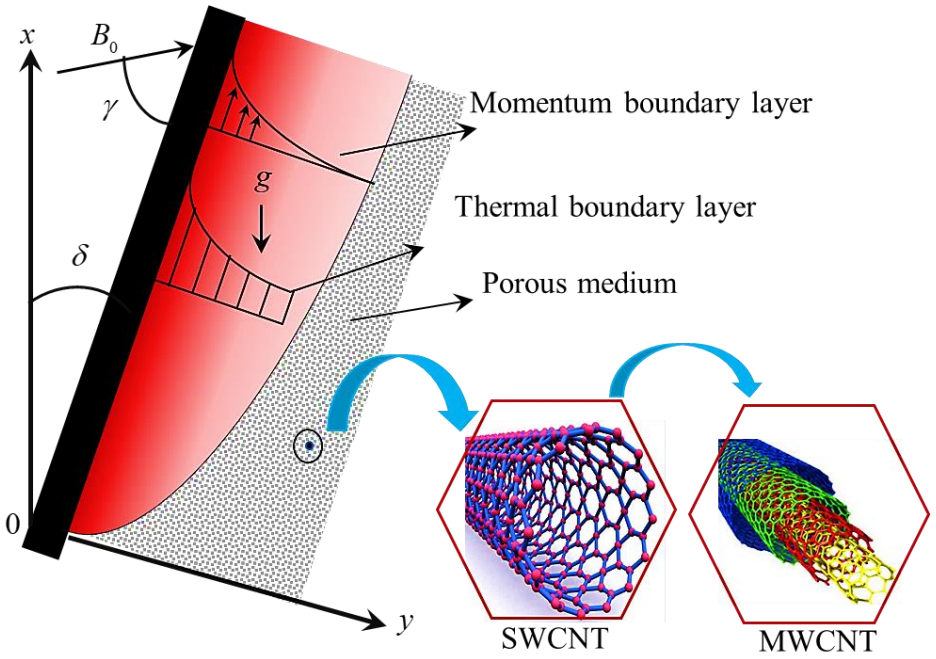

Figure 1 physical configuration and coordinates system

In the proposed problem the Casson fluid model is subjected to blood and CNts nanoparticles are dispersed into it for enhanced heat transfer. The rheological relation and Cauchy stress tension of Casson fluid is given as under [35,36]

Preprints (www.preprints.org) | NOT PEER-REVIEWED | Posted: 7 April 2020 doi:10.20944/preprints202004.0088.v1

Peer-reviewed version available at Symmetry 2020, 12, 768; doi:10.3390/sym12050768

$$\underline{\mathbf{T}} = \begin{cases} 2\left(\mu_B + \dfrac{p_r}{\sqrt{2\pi}}\right)e_{ij}, & \pi > \pi_c \\ 2\left(\mu_B + \dfrac{p_r}{\sqrt{2\pi_c}}\right)e_{ij}, & \pi < \pi_c \end{cases}, \tag{1}$$

where μ_B is the plastic dynamic viscosity, p_r is the yield stress and π_c is the critical values of the product of μ_B, and p_r. In the virtue of Eq. (1) along with momentum equation, Maxwell set of equations [37], Darcy's law [38], Fourier law of heat conduction [39] and Boussinesq approximation [40] the governing equations of the proposed problem as given by [36]

$$\rho_{nf}\frac{\partial u(y,t)}{\partial t} = \mu_{nf}\left(1+\frac{1}{\beta_0}\right)\frac{\partial^2 u(y,t)}{\partial y^2} - \left\{\sigma_{nf}B_0{}^2\sin\gamma + \left(1+\frac{1}{\beta_0}\right)\frac{\mu_{nf}\varphi}{k}\right\}u(y,t), \tag{2}$$
$$+g\left(\rho\beta_T\right)_{nf}\left(T(y,t)-T_\infty\right)\cos\delta$$

$$\left(\rho C_p\right)_{nf}\frac{\partial T(y,t)}{\partial t} = k_{nf}\frac{\partial^2 T(y,t)}{\partial y^2}, \tag{3}$$

subject to the following initial and boundary conditions

$$u(y,0) = 0, T(y,0) = T_\infty, \forall\, y \geq 0, \tag{4}$$

$$\left.\begin{array}{l} u(0,t) = U_0 H(t)\cos\omega t,\ T(0,t) = T_W, \text{for}\, t > 0 \\ u(y,t) \to 0, T(y,t) \to T_\infty;\ y \to \infty, \text{for}\, t > 0 \end{array}\right\}, \tag{5}$$

where ρ_{nf} is the density, $u(y,t)$ is the velocity, μ_{nf} is the dynamic viscosity, β_0 is the Casson fluid parameter, σ_{nf} is the electrical conductivity, $\varphi(0<\varphi<1)$ is the porosity, k is the permeability, g is the gravitational acceleration, β_T is the thermal expansion, $T(y,t)$ is the temperature, $\left(C_p\right)_{nf}$ is the heat capacitance and k_{nf} is the thermal conductivity. The subscript nf is used for nanofluid where the subscripts f and s will be used for base fluid and solid nanoparticles respectively. The mathematical models for the thermophysical properties of nanofluid are given in Table 1 whereas its numerical values are given in Table 2.

Preprints (www.preprints.org) | NOT PEER-REVIEWED | Posted: 7 April 2020 doi:10.20944/preprints202004.0088.v1

Peer-reviewed version available at Symmetry 2020, 12, 768; doi:10.3390/sym12050768

Table 1 Mathematical model for thermophysical properties of nanofluid [41].

Physical Quantity	Mathematical model
Density	$\rho_{nf} = (1-\phi)\rho_f + \phi\rho_s$
Dynamic viscosity	$\mu_{nf} = \dfrac{\mu_f}{(1-\phi)^{2.5}}$
Electrical conductivity	$\sigma_{nf} = \left\{1 + \dfrac{3\left(\frac{\sigma_s}{\sigma_f} - 1\right)\phi}{\left(\frac{\sigma_s}{\sigma_f} + 2\right) - \left(\frac{\sigma_s}{\sigma_f} - 1\right)\phi}\right\}\sigma_f$
Thermal expansion	$(\rho\beta_T)_{nf} = (1-\phi)(\rho\beta_T)_f + \phi(\rho\beta_T)_s$
Heat capacitance	$(\rho C_p)_{nf} = (1-\phi)(\rho C_p)_f + \phi(\rho C_p)_s$
Thermal conductivity	$k_{nf} = \left\{\dfrac{(1-\phi) + 2\phi\frac{k_s}{k_s - k_f}\ln\frac{k_s - k_f}{2k_f}}{(1-\phi) + 2\phi\frac{k_s}{k_s - k_f}\ln\frac{k_s + k_f}{2k_f}}\right\}k_f$

Table 2 Numerical values of thermophysical properties of base fluid and nanoparticles [36]

Material	Base fluid	Nanoparticles	
	Human blood	SWCNTs	MWCMTs
$\rho(\mathrm{kg/m^3})$	1053	2600	1600
$C_p(\mathrm{J/kg\,K})$	3594	425	796
$k(\mathrm{W/m\,K})$	0.492	6600	3000
$\beta_T \times 10^{-5}(K^{-1})$	0.8	$10^{-6} - 10^{-7}$	1.9×10^{-4}
σ	0.18	21	44

3. Methodology

In this study, the Laplace transform is used to acquire exact solutions of the considered problem. Primarily, the proposed model is transformed to dimensionless form with an eye to reduce the number of variables and eradicate unite for clarity. Then the dimensionless governing

Preprints (www.preprints.org) | NOT PEER-REVIEWED | Posted: 7 April 2020 doi:10.20944/preprints202004.0088.v1

Peer-reviewed version available at Symmetry 2020, 12, 768; doi:10.3390/sym12050768

equations are artificially transformed to time-fractional Atangana- Baleanu fractional derivatives. The Atangana-Baleanu fractional Casson nanofluid model is dealt with the Laplace transform technique to generate exact solutions for velocity and temperature profiles. The obtained results are displayed in numerous graphs and discussed physically.

Description of the operational framework.

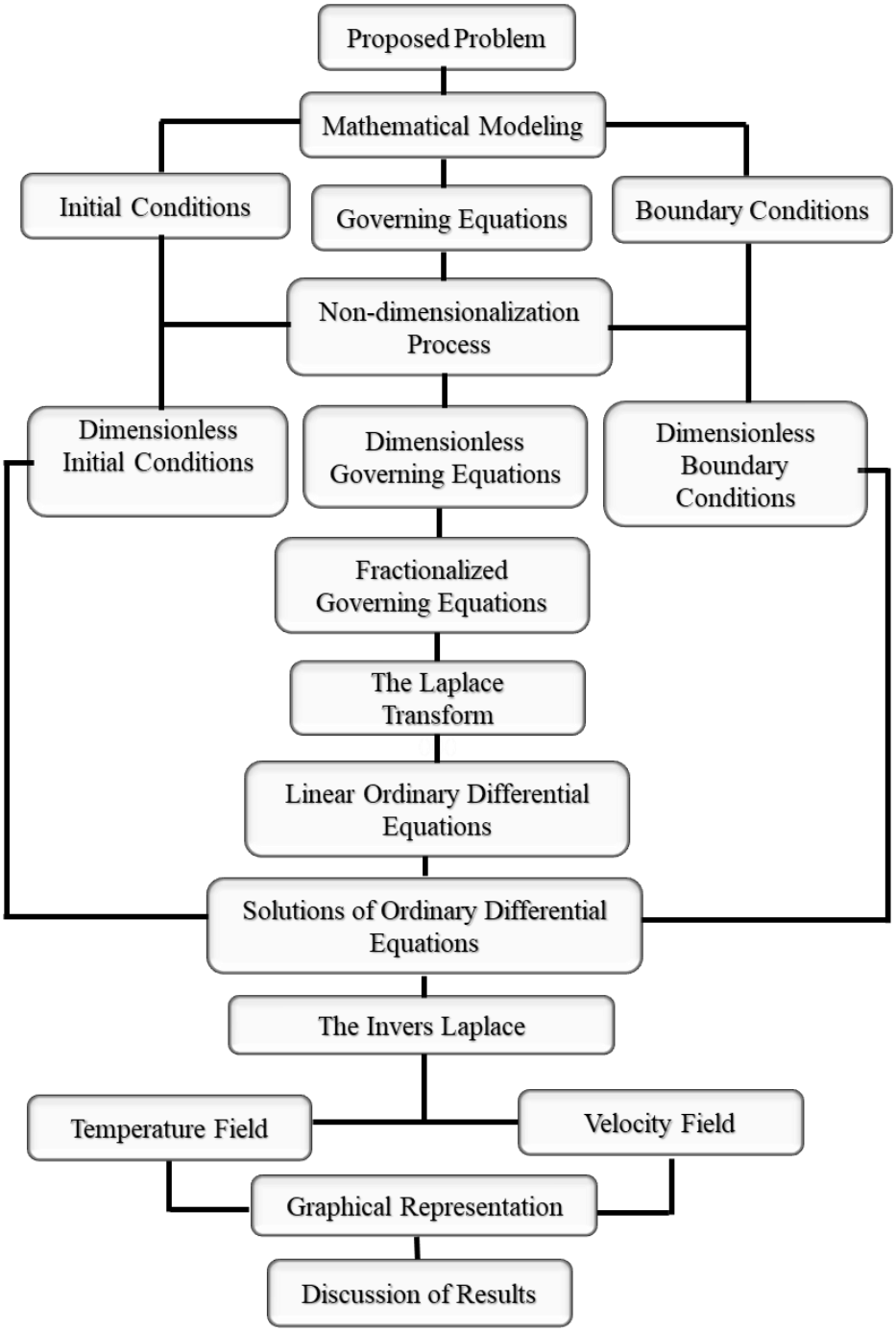

Preprints (www.preprints.org) | NOT PEER-REVIEWED | Posted: 7 April 2020 doi:10.20944/preprints202004.0088.v1

Peer-reviewed version available at Symmetry 2020, 12, 768; doi:10.3390/sym12050768

Now, incorporate the following dimensionless variables

$$u^* = \frac{u}{u_0},\ y^* = \frac{u_0}{\upsilon_f}, t^* = \frac{u_0^{\ 2}}{\upsilon_f} t, \theta = \frac{T - T_\infty}{T_W - T_\infty}$$

into Eqs. (2)-(5) yield to

$$\phi_0 \frac{\partial u(y,t)}{\partial t} = \frac{\phi_1}{\beta} \frac{\partial^2 u(y,t)}{\partial y^2} - \left(\phi_2 M \sin\gamma + \frac{\phi_3}{K} \right) u(y,t) + \phi_4 Gr\theta(y,t)\cos\delta, \tag{6}$$

$$\phi_5 \Pr \frac{\partial \theta(y,t)}{\partial t} = \phi_6 \frac{\partial^2 \theta(y,t)}{\partial y^2}, \tag{7}$$

$$t \le 0 : u(y,0) = 0, \theta(y,0) = 0, \forall y \ge 0, \tag{8}$$

$$\left.\begin{array}{l} u(0,t) = H(t)\cos\omega t,\ \theta(0,t) = 1, \text{for } t > 0 \\ u(y,t) \to 0, \theta(y,t) \to 0;\ t \to \infty, \text{for } t > 0 \end{array}\right\}, \tag{9}$$

where

$$\beta = \frac{\beta_0}{1+\beta_0},\ M = \frac{\nu_f \sigma_f B_0^{\ 2}}{\rho_f U_0^{\ 2}}, K = \frac{k u_0^2}{\upsilon_f \varphi}\ Gr = \frac{g(\upsilon\beta_T)_f (T_W - T_\infty)}{u_0^{\ 3}},\ \Pr = \left(\frac{\mu C_p}{k} \right)_f$$

$$\phi_0 = (1-\phi_{nf}) + \frac{\phi\rho_s}{\rho_f},\ \phi_1 = \frac{1}{1-\phi},\ \phi_2 = \frac{\sigma_{hnf}}{\sigma_f},\ \phi_3 = (1-\phi) + \frac{\phi(\rho\beta_T)_s}{(\rho\beta_T)_f},$$

$$\phi_4 = (1-\phi) + \frac{\phi(\rho C_p)_s}{(\rho C_p)_f},\ \phi_5 = \frac{k_{nf}}{k_f}$$

is the dimensionless Casson fluid parameter, magnetic number, permeability parameter, thermal Grashof number, and Prandtl number respectively and ϕ_0, ϕ_1, ϕ_2, ϕ_3, ϕ_4, and ϕ_5 are constant terms produced during Calculi. The time-fractional form of Eqs. (6) and (7) is given by [42,43]

$$\phi_0\ {}^{AB}\mathcal{D}_t^{\alpha} u(y,t) = \frac{\phi_1}{\beta} \frac{\partial^2 u(y,t)}{\partial y^2} - \left(\phi_2 M \sin\gamma + \frac{\phi_1}{K} \right) u(y,t) + \phi_3 Gr\theta(y,t)\cos\delta; 0 < \alpha \le 1, \tag{10}$$

$$\phi_4 \Pr\ {}^{AB}\mathcal{D}_t^{\alpha} \theta(y,t) = \phi_5 \frac{\partial^2 \theta(y,t)}{\partial y^2}; 0 < \alpha \le 1, \tag{11}$$

where ${}^{AB}\mathcal{D}_t^{\alpha}(.,.)$ is the Atangana-Baleanu time-fractional operator defined by [34]

Preprints (www.preprints.org) | NOT PEER-REVIEWED | Posted: 7 April 2020 doi:10.20944/preprints202004.0088.v1

Peer-reviewed version available at Symmetry 2020, 12, 768; doi:10.3390/sym12050768

$$ {}^{AB}\mathcal{D}_{\tau}^{\alpha} f(\eta,\tau) = \frac{N(\alpha)}{1-\alpha}\int_0^{\tau} E_{\alpha}\left\{\frac{-\alpha(\tau-t)^{\alpha}}{1-\alpha}\right\} f'(\eta,\tau)\,dt; 0<\alpha\le 1, \tag{12} $$

where

$$ E_{\alpha}\left(-t^{\alpha}\right) = \sum_{K=0}^{\infty}\frac{(-t)^{\alpha K}}{\Gamma(\alpha K+1)} \tag{13} $$

is the non-local and non-singular Mittag-Leffler function used as the kernel in the construction of Eq. (12). The Laplace transform of Eq. (12) is given by [44]

$$ \mathcal{L}\left\{f(\eta,\tau);q\right\} = \frac{q^{\alpha}\mathcal{L}\left\{f(\eta,\tau)\right\} - f(\eta,0)}{(1-\alpha)q^{\alpha}+\alpha}; 0<\alpha\le 1 \tag{14} $$

where $\mathcal{L}\left\{f(\eta,\tau)\right\} = \bar{f}(\eta,q)$ is the $f(\eta,\tau)$ in the Laplace transform domain and $f(\eta,0)$ is the initial values of $f(\eta,\tau)$. It worth mentioning here that for $\alpha=1$, the model presented in Eqs (10) and (11) is reduced back to the classical form exhibited in Eqs. (2) and (3). This validated the time-fractional model proposed for CNT's-blood nanofluid.

4. Solutions of the Problem

The Laplace transform technique is adopted to find the exact solutions for the proposed problem.

4.1 Solution of Energy Equation

Applying the Laplace transform to Eq. (11) in the light of Eqs. (12) and (14) and using the corresponding initial and boundary conditions from Eqs. (8) and (9) yield to

$$ \frac{\partial^2\bar{\theta}(y,q)}{\partial y^2} - \frac{\phi_4\,\mathrm{Pr}}{\phi_5}\frac{q^{\alpha}\bar{\theta}(y,q)}{(1-\alpha)q^{\alpha}+\alpha} = 0; 0<\alpha\le 1. \tag{15} $$

The analytical solution of the homogeneous Eq. (15) is given by

$$ \bar{\theta}(y,q) = \frac{1}{q}\exp\left(-y\sqrt{\frac{\phi_4\,\mathrm{Pr}}{\phi_5}\frac{q^{\alpha}}{(1-\alpha)q^{\alpha}+\alpha}}\right); 0<\alpha\le 1. \tag{16} $$

Equations (16) is written in a more convenient form as

$$ \bar{\theta}(y,q) = \bar{\chi}(q)\bar{\psi}(\xi,q;a_2,a_3); 0<\alpha\le 1, \tag{17} $$

Preprints (www.preprints.org) | NOT PEER-REVIEWED | Posted: 7 April 2020 doi:10.20944/preprints202004.0088.v1

Peer-reviewed version available at Symmetry 2020, 12, 768; doi:10.3390/sym12050768

where

$$\bar{\psi}\left(y,q;a_2,a_3\right)=\frac{1}{q^{\alpha}}\exp\left(-y\sqrt{\frac{a_2q^{\alpha}}{q^{\alpha}+a_3}}\right), \tag{18}$$

$$\bar{\chi}\left(q\right)=\frac{1}{q^{1-\alpha}}.., \tag{19}$$

and

$$a_0=\frac{\phi_4\,\mathrm{Pr}}{\phi_5},\ a_1=\frac{1}{1-\alpha},\ a_2=a_0a_1,\ a_3=a_1\alpha$$

The solution of the energy equation in the Laplace transform domain is given in Eq. (17). Applying the inverse Laplace transform to Eq. (17) yield to

$$\theta\left(y,t\right)=\int_0^t\chi\left(t-\tau\right)\psi\left(y,\tau;a_2,a_3\right)d\tau;0<\alpha\le1, \tag{20}$$

Equation (20) represents the final solutions of the energy equation in terms of convolution product where

$$\psi\left(y,t;a_2,a_3\right)=\mathcal{L}^{-1}\left\{\bar{\psi}\left(y,q;a_2,a_3\right)\right\}=$$
$$\frac{1}{\pi}\int_0^{\infty}\int_0^{\infty}\left(ur^{\alpha}\sin\alpha\pi\right)\psi_1\left(y,t;a_2,a_3\right)\exp\left(-\tau r-ur^{\alpha}\cos\alpha\pi\right)drdu, \tag{21}$$

$$\psi_1\left(y,t;a_2,a_3\right)=\mathcal{L}^{-1}\left\{\frac{1}{q}\exp\left(-y\sqrt{\frac{a_2q}{q+a_3}}\right)\right\}=1-\frac{2a_2}{\pi}\int_0^{\infty}\frac{\sin(ys)}{s\left(a_2+s^2\right)}\exp\left(-\frac{a_3ts^2}{a_2+s^2}\right)ds, \tag{22}$$

and

$$\chi\left(t\right)=\frac{1}{t^{\alpha}\Gamma\left(1-\alpha\right)}, \tag{23}$$

It is mentionable here that Eq. (20) satisfy all the imposed physical conditions which validate our solutions.

4.2 Solutions of Momentum Equation

In this section, the same procedure of solutions as of energy equation is acquired. The Laplace transform technique is applied to Eq. (10) and the corresponding initial conditions are used from

Preprints (www.preprints.org) | NOT PEER-REVIEWED | Posted: 7 April 2020 doi:10.20944/preprints202004.0088.v1

Peer-reviewed version available at Symmetry 2020, 12, 768; doi:10.3390/sym12050768

Eq. (8) which yield to the following nonhomogeneous differential equation in the Laplace transform domain

$$\frac{d^2\bar{u}(y,q)}{dy^2}-\left(\frac{b_2q^{\alpha}+b_3}{q^{\alpha}+a_3}\right)\bar{u}(y,q)=-\frac{b1}{q}\exp\left(-y\sqrt{\frac{a_2q^{\alpha}}{q^{\alpha}+a_3}}\right);0<\alpha\le 1, \tag{24}$$

where

$$b_1=\frac{\beta\phi_3Gr\cos(\delta)}{\phi 1}=\frac{\beta_0\phi_0a_1}{\phi_1},b_2=K_{eff}+b_0,K_{eff}=\frac{\beta\phi_2M\sin\gamma}{\phi_1}+\frac{\beta}{K},\ b_0=\frac{\beta_0\phi_0a_1}{\phi_1},b_3=K_{eff}a_2\,.$$

The exact analytical solutions of Eq. (24) is given by

$$\begin{aligned}\bar{u}(y,q)=&\frac{q}{q^2+\omega^2}\exp\left(-y\sqrt{\frac{b_2q^{\alpha}+b_3}{q^{\alpha}+a_3}}\right)+\left\{b_1\left(\frac{q^{\alpha}+a_3}{b_4q^{\alpha}-b_3}\right)\right\}\\&\left\{\frac{1}{q}\exp\left(-y\sqrt{\frac{b_2q^{\alpha}+b_3}{q^{\alpha}+a_3}}\right)-\frac{1}{q}\exp\left(-y\sqrt{\frac{a_2q^{\alpha}}{q^{\alpha}+a_3}}\right)\right\};0<\alpha\le 1\end{aligned} \tag{25}$$

where

$$b_4=a_2-b_2\,.$$

Equation (25) is written in an additional simplified and convenient form as

$$\begin{aligned}\bar{u}(\xi,q)=&\frac{q}{q^2+\omega^2}\times q\bar{\chi}(q)\bar{\Phi}(y,q,b_2,b_3,a_3)+b_1\left(\frac{q^{\alpha}}{b_4q^{\alpha}-b_3}+\frac{b_1}{b_4q^{\alpha}-b_3}\right).\\&\times\left\{\bar{\chi}(q)\bar{\Phi}(y,q,b_2,b_3,a_3)-\bar{\theta}(y,q)\right\};0<\alpha\le 1\end{aligned} \tag{26}$$

where

$$\bar{\Phi}(y,q,b_2,b_3,a_3)=\frac{1}{q}\exp\left(-y\sqrt{\frac{b_2q+b_3}{q+a_3}}\right). \tag{27}$$

Upon taking the inverse Laplace to transform Eq. (26) takes the following form

$$\begin{aligned}u(y,t)=&\cos(\omega t)*\Phi(y,t,b_2,b_3,a_3)+\frac{b_1}{b_4}\left\{R_{\alpha,\alpha}\left(\frac{b_3}{b_4},t\right)+b_1F_{\alpha}\left(\frac{b_3}{b_4},t\right)\right\},\\&*\left\{\chi(t)\Phi(y,t,b_2,b_3,a_3)-\theta(y,t)\right\};0<\alpha\le 1\end{aligned} \tag{28}$$

Preprints (www.preprints.org) | NOT PEER-REVIEWED | Posted: 7 April 2020 doi:10.20944/preprints202004.0088.v1

Peer-reviewed version available at Symmetry 2020, 12, 768; doi:10.3390/sym12050768

where $\theta(y,t)$ is presented in Eqs. (20)-(23) and $R_{\alpha,\upsilon}(.,.)$ is the Lorenzo and Hartleys function and $F_{\alpha}(.,.)$ Robotnov and Hartleys' function defined by which are given by [37]

$$R_{\alpha,\upsilon}(-m,t)=\left(\frac{q^{\upsilon}}{q^{\alpha}+m}\right)=\sum_{n=0}^{\infty}\frac{(-m)^{n}\,t^{(n+1)\alpha-1-\upsilon}}{\Gamma\{(n+1)\alpha-\upsilon\}}, \tag{29}$$

$$F_{\alpha}(-m,t)=\left(\frac{1}{q^{\alpha}+m}\right)=\sum_{n=0}^{\infty}\frac{(-m)^{n}\,t^{(n+1)\alpha-1}}{\Gamma\{(n+1)\alpha\}}. \tag{30}$$

and the newly established function $\Phi(y,t,b_2,b_3,a_3)$ is given by

$$\begin{aligned}\Phi(y,t,b_2,b_3,a_3)&=\mathcal{L}^{-1}\left\{\bar{\Phi}(y,q,b_2,b_3,a_3)\right\}=\\&\frac{1}{\pi}\int_0^{\infty}\int_0^{\infty}\left(ur^{\alpha}\sin(\alpha\pi)\right)\Phi_1(y,t,b_2,b_3,a_3)\exp\left(-tr-ur^{\alpha}\cos(\alpha\pi)\right)drdu,\end{aligned} \tag{31}$$

where

$$\begin{aligned}\Phi_1(y,t,b_2,b_3,a_3)&=\mathcal{L}^{-1}\left\{\frac{1}{q}\exp\left(-y\sqrt{\frac{b_2q+b_3}{q+a_3}}\right)\right\}=\exp\left(-y\sqrt{b_2}\right)\\&-\int_0^{\infty}\int_0^{\tau}\frac{y\sqrt{b_3-b_2a_3}}{2(\pi s)^{\frac{1}{2}}}\exp(a_3s)\times\frac{1}{u}\exp\left(-\frac{y^2}{4u}-b_2u\right)I_1\left\{2\left(u(b_3-b_2a_3)s\right)^{\frac{1}{2}}\right\}duds,\end{aligned} \tag{32}$$

and $I_1(.)$ is the Bessel function of the first kind. Equations (20) and (31) complete the solutions of the assumed problem. These solutions are additional reliable, flexible and generalized which will be discussed in the up forth section in detail with a physical explanation.

5. Discussion of Results

In this section, the effects of various flow parameters (for instance, fractional parameter α, the volume concentration of CNTs ϕ, Casson fluid parameter β, magnetic parameter M, angle of inclination of the magnetic field γ, the permeability of porous medium K and thermal Garshof number Gr) are characterized in multiple figures (Figures 2-11) on temperature and velocity profiles. For the human blood, the Prandtl number is chosen 21 and the impact of all the above-stated parameters is displayed for human blood-SWCNTs and human blood-MWCNs.

Figures (2) and (3) are outlined to display the implications of α on temperature and velocity profiles. These figures turn out that the temperature and velocity profiles are declining for increasing values of α in both the cases (blood-SWCNTs and human blood-MWCNs.). The physical point is the higher values of α relating to the thickness of thermal and momentum boundary layers. Higher the values of α, deducing the thickness of the thermal boundary layer for that reason the temperature and velocity profiles evidence a decreasing tendency. The trend can be defended from the published work of Ali et al. [40,45]. Besides this, the region of temperature and velocity profiles for $0 < \alpha \leq 1$ is the memory of Atangana-Baleanu fractional derivative which leads to generality and flexibility of the results. By fixing the values of α the desired results can be achieved.

The repercussions of ϕ on temperature and velocity profiles are reported in figures (4) and (5) for SWCNTs and MWCNTs. The conduct of velocity and temperature profiles is reversed. This is in the view of thermal conductivities and densities depicted in Tables (1) and (2). The temperature profile involved only thermal conductivities; however, the velocity profile implicates both densities and thermal conductivities because the energy equation (Eq. (3)) is partially coupled with momentum equations (Eq.(2)). For $\phi = 0.01, 0.02, 0.03, 0.04$ cause increment in the thermal conductivity of nanofluids (SWCNTs and MWCNTs nanofluids) consequently the temperature profile increase. In the case of the velocity profile, the density dominates the thermal conductivities and for $\phi = 0.01, 0.02, 0.03, 0.04$ the nanofluids became denser and viscous accordingly the velocity profile decelerated as presented in the published work [16,46]. In addition, Figure (6) is plotted to equate SWCNTs and MWCNTs in temperature and velocity profiles. This figure clearly justifies the behavior in figures (4) and (5).

Figure (7) display the impact of β on the velocity profile. Increasing β reducing the motion of CNTs nanofluid because of the reduction in the momentum boundary layer. Figure (8) disclose the impact of M on the velocity profile for both SWCNTs and MWCNTs. The M is a dimensionless number which is accorded with the Lorentz force that counters the nanofluid velocity. Higher the M higher will be the Lorentz force which will resist the motion. This is why the velocity retarded in both the cases of CNTs with increasing M [42]. Likewise, the inclination of the magnetic field γ weakens the impact of M that carries off the Lorentz force.

Preprints (www.preprints.org) | NOT PEER-REVIEWED | Posted: 7 April 2020 doi:10.20944/preprints202004.0088.v1

Peer-reviewed version available at Symmetry 2020, 12, 768; doi:10.3390/sym12050768

For $\gamma = \pi/2$ (normal magnetic field) the influence of the Lorentz force is the strongest as depicted in Figure (9) [43].

Figure (10) presents the effect of K on the velocity profile for both the cases of CNTs. It is witnessed that greater values of K magnifying the velocity field. This is on account of a reduction of resistance of porous medium and causes improvement in the momentum boundary layer. Physically, in this view, the velocity field enhanced [38]. Finally, Figure (11) depicts the consequences of Gr on the velocity profile. it is the ratio of buoyancy and viscous forces. The higher Gr leads to enhancement in buoyancy forces that give grow the induced flows [35].

6. Concluding Remarks

In the study, a fractional initial and boundary values problem is modeled for the flow of human blood-CNTs nanofluid over an inclined plate. The effects of an inclined magnetic field and saturated porous medium are considered. The exact analytical solutions for temperature and velocity fields are drafted via the Laplace transform technique. The exact solutions are displayed in various graphs and discussed with physical arguments. The main finding extracted from this study are as follow:

- The fractional solutions for temperature and velocity fields are more general, reliable, flexible having memory and heredity property which can be numerically reduced for any values of $0 < \alpha \leq 1$.
- The temperature profile increase with an increasing volume fraction of CNTs although decreases with increasing fractional parameter (for both cases of CNTs) because of variation in the thermal boundary layer.
- The velocity profile increases with increased permeability of the porous medium and thermal Grashof number due to the improvement in the velocity boundary layer.
- The nanofluids motion (SWCNTs and MWCTs) retarded with increment in volume concentration of CNTs, magnetic parameters. The normal magnetic field has the strongest resistance to the motion.
- The trends and features of all the physical flow parameters are in excellent agreement with the published work.

Competing interest

All the authors declared that there is no competing interest regarding this manuscript

Acknowledgment

The authors would like to acknowledge Ministry of Education (MOE) and Research Management Centre-UTM, Universiti Teknologi Malaysia (UTM) for the financial support through vote numbers 5F004, 07G70, 07G72, 07G76, 07G77 and 08G33 for this research

Preprints (www.preprints.org) | NOT PEER-REVIEWED | Posted: 7 April 2020 doi:10.20944/preprints202004.0088.v1

Peer-reviewed version available at Symmetry 2020, 12, 768; doi:10.3390/sym12050768

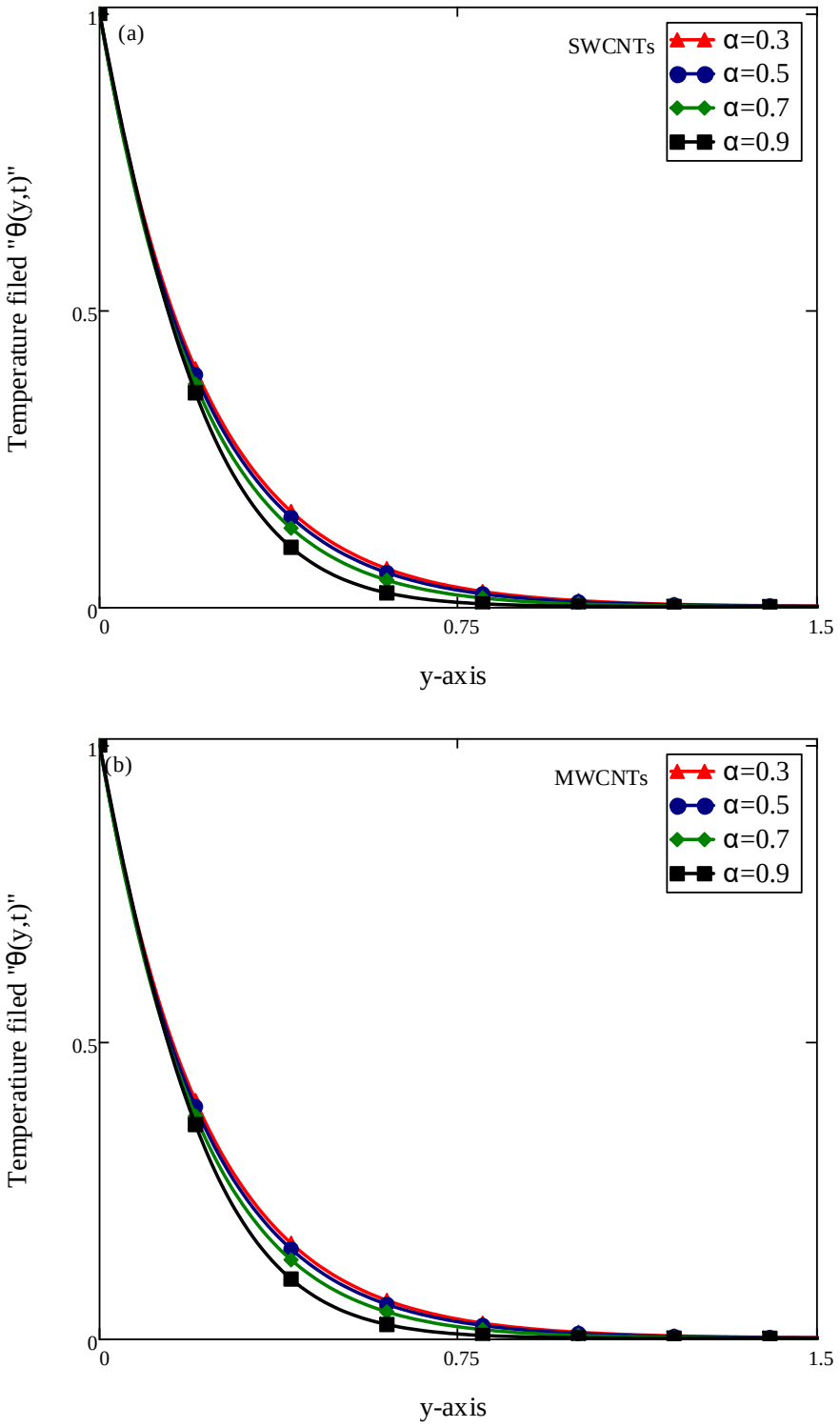

Figure 2 *Consequences of* α *on* $\theta(y,t)$ *when* $t = 0.5$, $\Pr = 21$ *and* $\phi = 0.04$

Preprints (www.preprints.org) | NOT PEER-REVIEWED | Posted: 7 April 2020 doi:10.20944/preprints202004.0088.v1

Peer-reviewed version available at Symmetry 2020, 12, 768; doi:10.3390/sym12050768

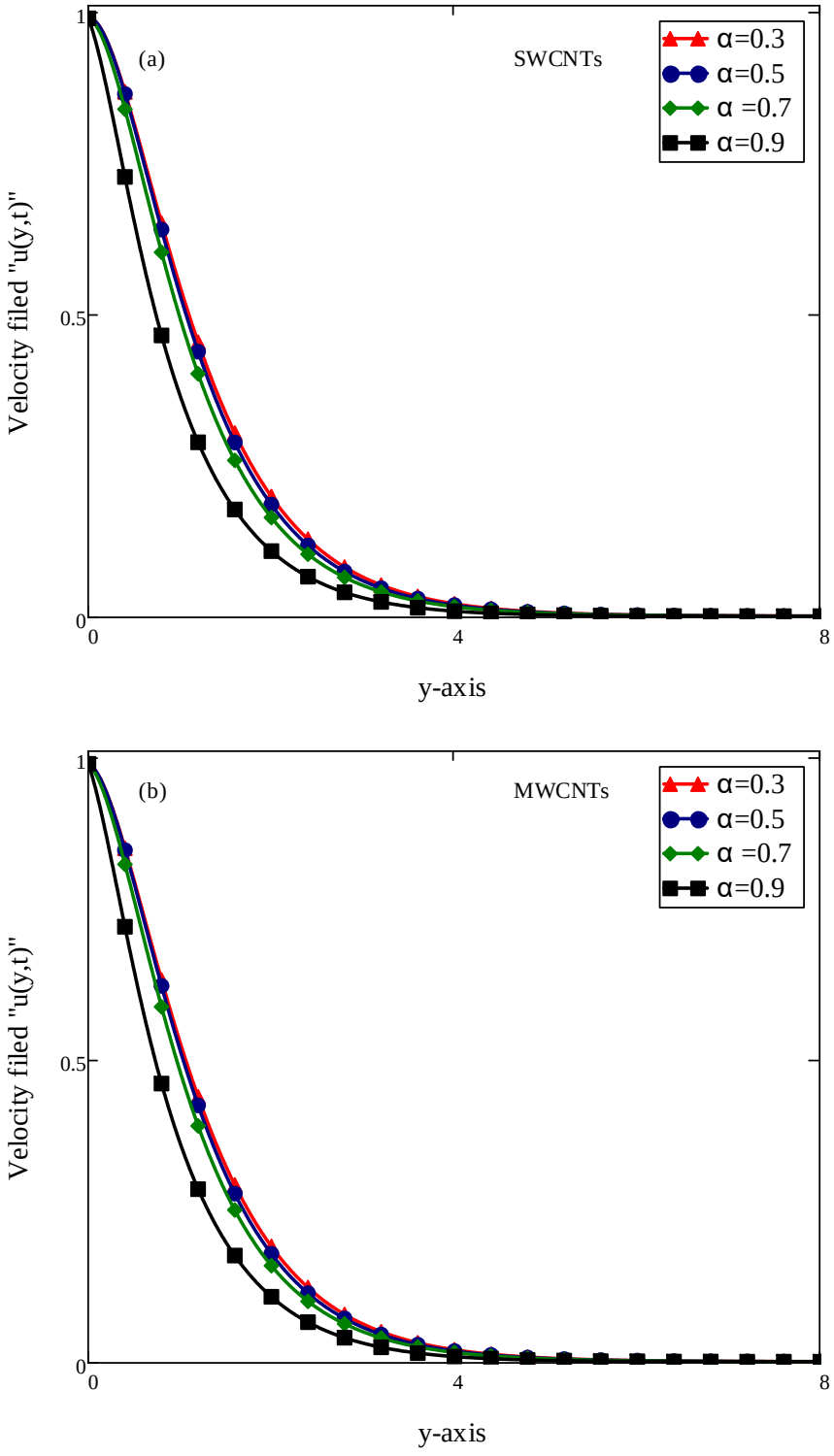

Figure 3 *Consequences of* α *on* $u(y,t)$ *when* $t=0.5$, $\beta=0.5$, $M=0.5$, $\gamma=\pi/2$, $K=0.5$ $Gr=7.0$, $\Pr=21$ *and* $\phi=0.04$

Preprints (www.preprints.org) | NOT PEER-REVIEWED | Posted: 7 April 2020 doi:10.20944/preprints202004.0088.v1

Peer-reviewed version available at Symmetry 2020, 12, 768; doi:10.3390/sym12050768

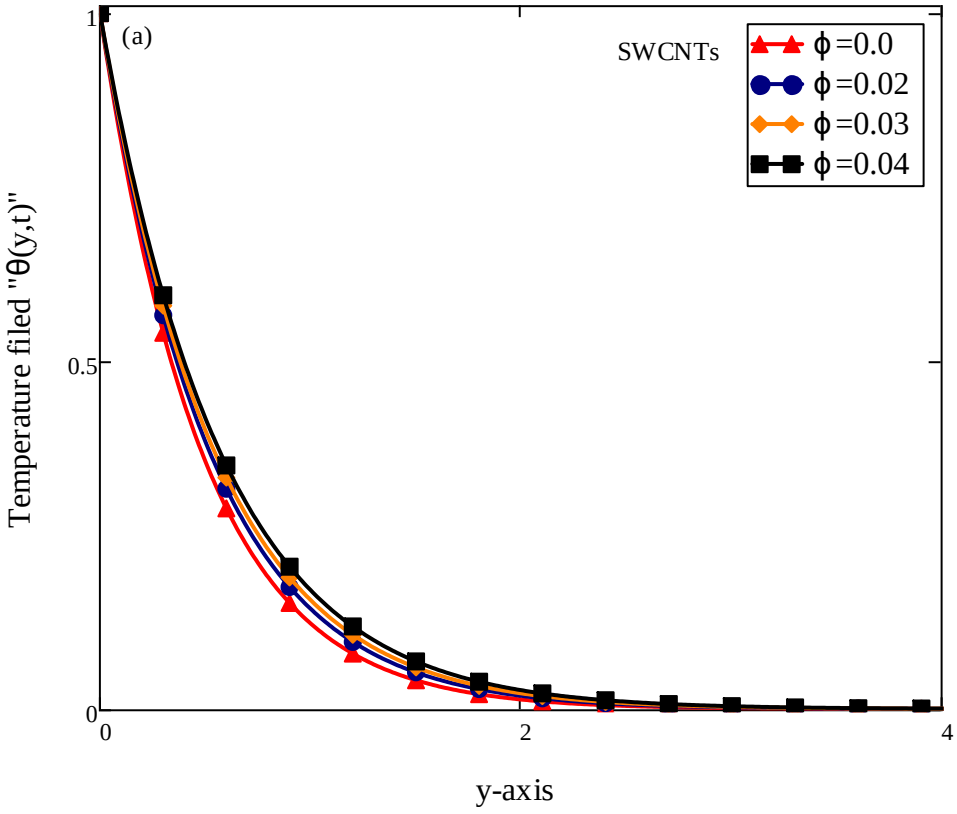

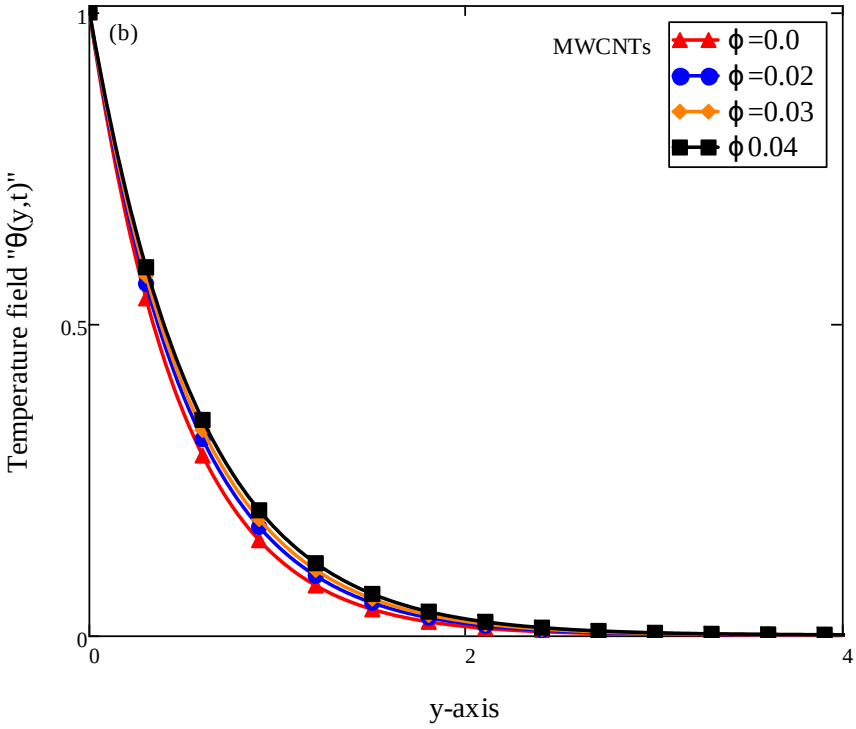

Figure 4 *Consequences of* ϕ *on* $\theta(y,t)$ *when* $t=0.5$, $\Pr=21$ *and* $\alpha=0.5$

Preprints (www.preprints.org) | NOT PEER-REVIEWED | Posted: 7 April 2020 doi:10.20944/preprints202004.0088.v1

Peer-reviewed version available at Symmetry 2020, 12, 768; doi:10.3390/sym12050768

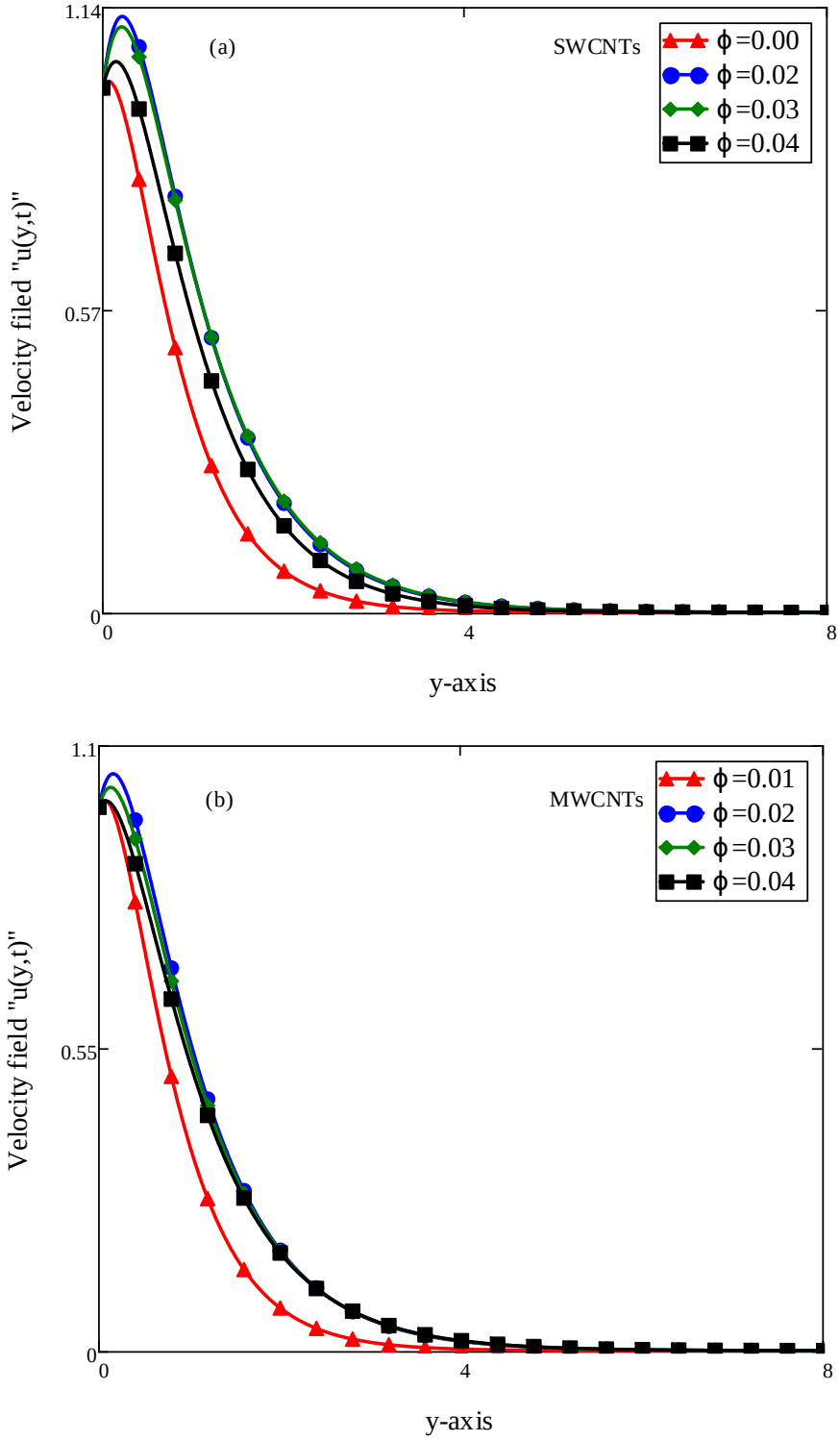

Figure 5 *Consequences of* ϕ *on* $u(y,t)$ *when* $t=0.5$, $\beta=0.5$, $M=0.5$, $\gamma=\pi/2$, $K=0.5$ $Gr=7.0$, $\Pr=21$ *and* $\alpha=0.5$

Preprints (www.preprints.org) | NOT PEER-REVIEWED | Posted: 7 April 2020 doi:10.20944/preprints202004.0088.v1

Peer-reviewed version available at Symmetry 2020, 12, 768; doi:10.3390/sym12050768

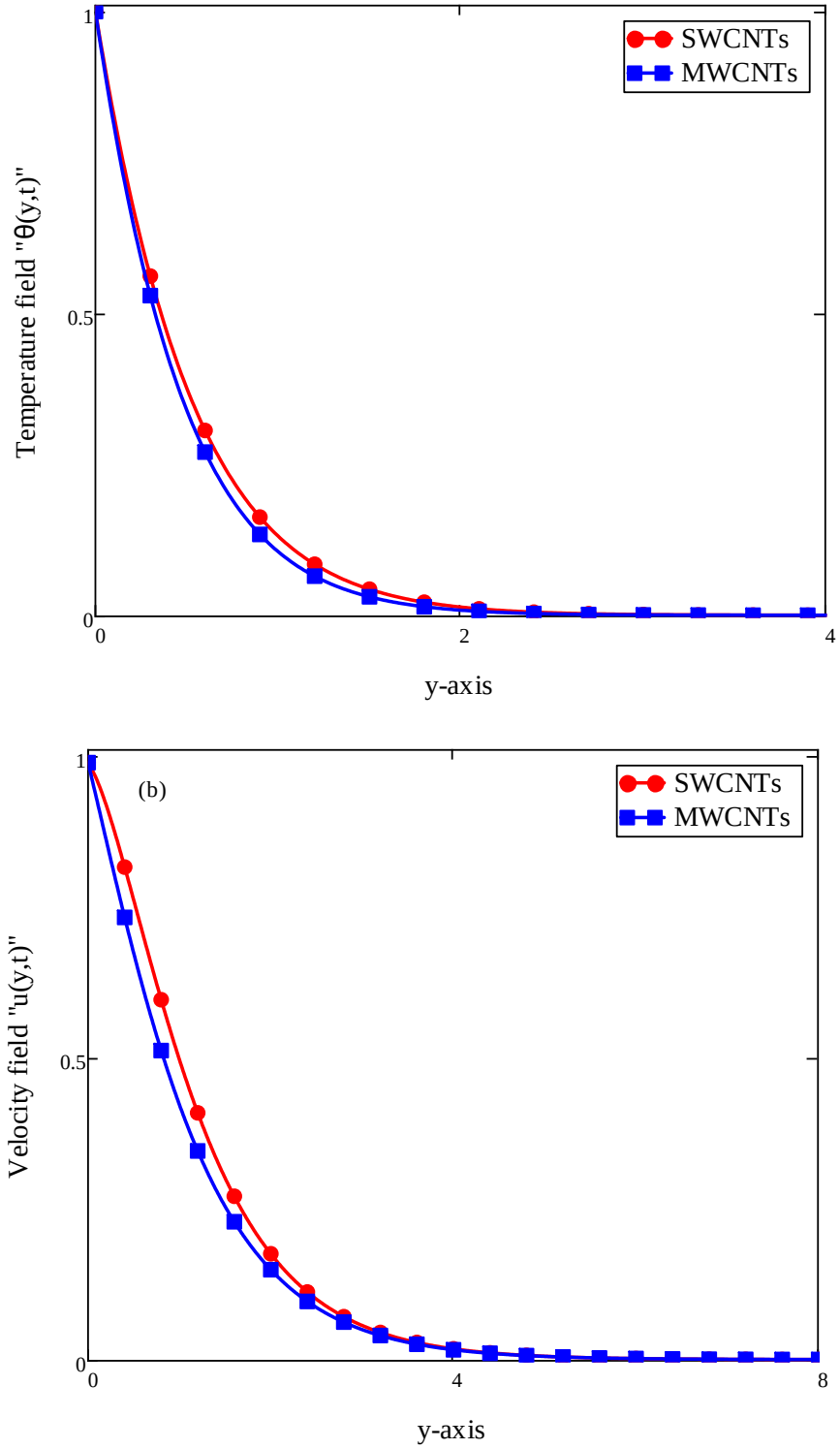

Figure 6 *comparison of* $\theta(y,t)$ *and* $u(y,t)$ *for SWCNTs and MWCNTs*

Preprints (www.preprints.org) | NOT PEER-REVIEWED | Posted: 7 April 2020 doi:10.20944/preprints202004.0088.v1

Peer-reviewed version available at Symmetry 2020, 12, 768; doi:10.3390/sym12050768

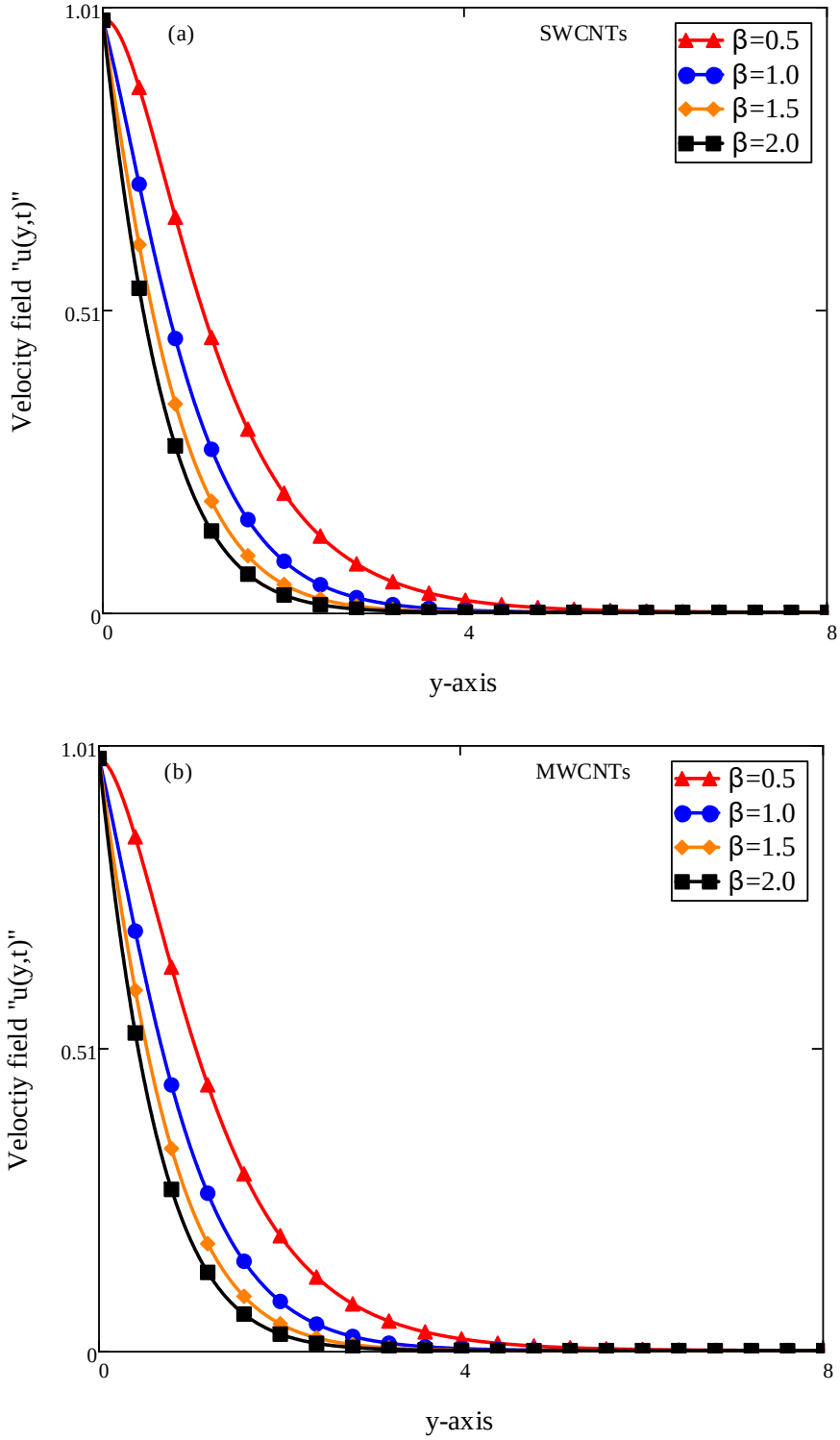

Figure 7 *Consequences of* β *on* $u(y,t)$ *when* $t=0.5$, $\phi=0.04$, $M=0.5$, $\gamma=\pi/2$, $K=0.5$ $Gr=7.0$, $\Pr=21$ *and* $\alpha=0.5$

Preprints (www.preprints.org) | NOT PEER-REVIEWED | Posted: 7 April 2020 doi:10.20944/preprints202004.0088.v1

Peer-reviewed version available at Symmetry 2020, 12, 768; doi:10.3390/sym12050768

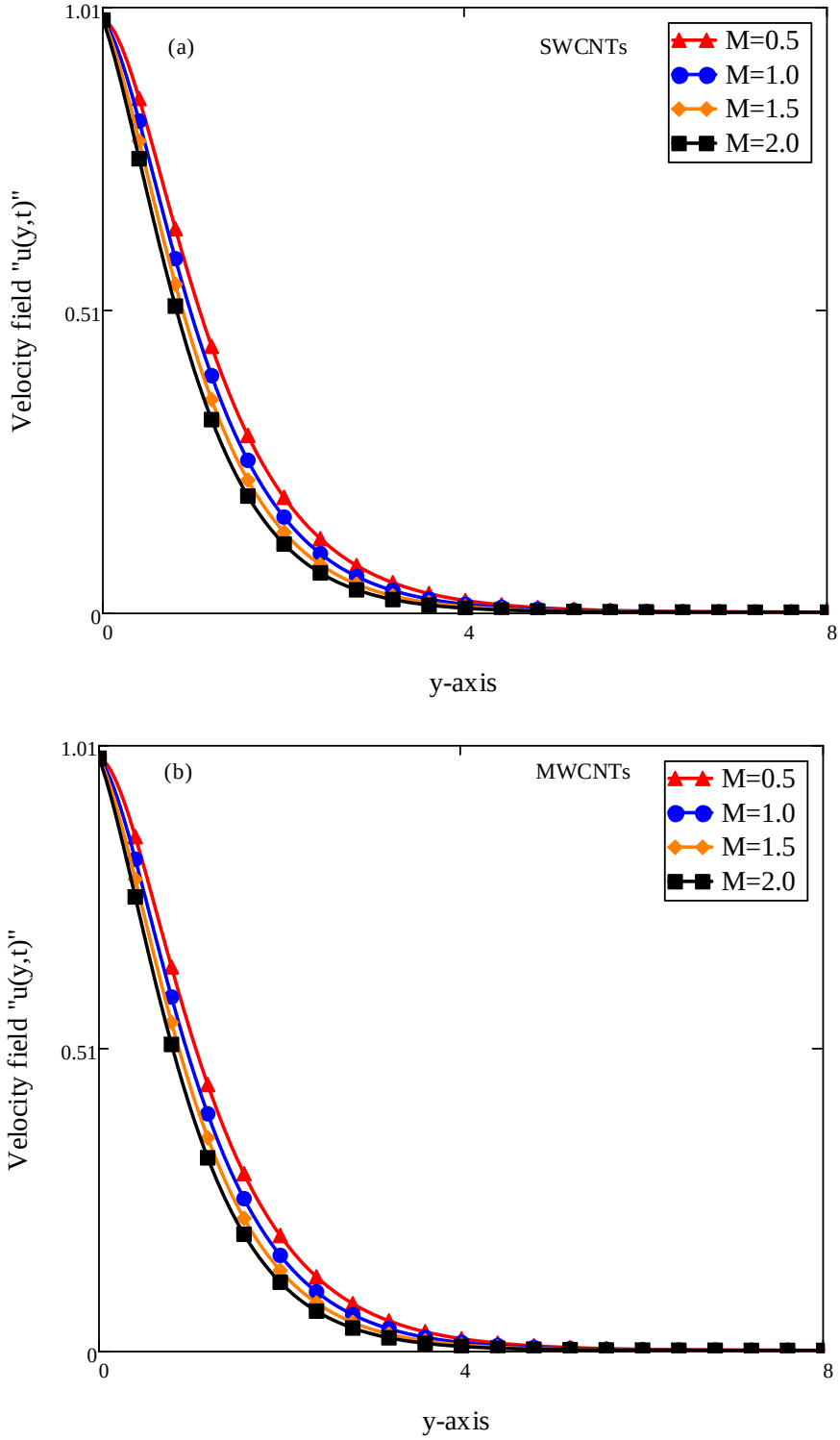

Figure 8 *Consequences of* M *on* $u(y,t)$ *when* $t=0.5$, $\beta=0.5$, $\phi=0.04$, $\gamma=\pi/2$, $K=0.5$ $Gr=7.0$, $\Pr=21$ *and* $\alpha=0.5$

Preprints (www.preprints.org) | NOT PEER-REVIEWED | Posted: 7 April 2020 doi:10.20944/preprints202004.0088.v1

Peer-reviewed version available at Symmetry 2020, 12, 768; doi:10.3390/sym12050768

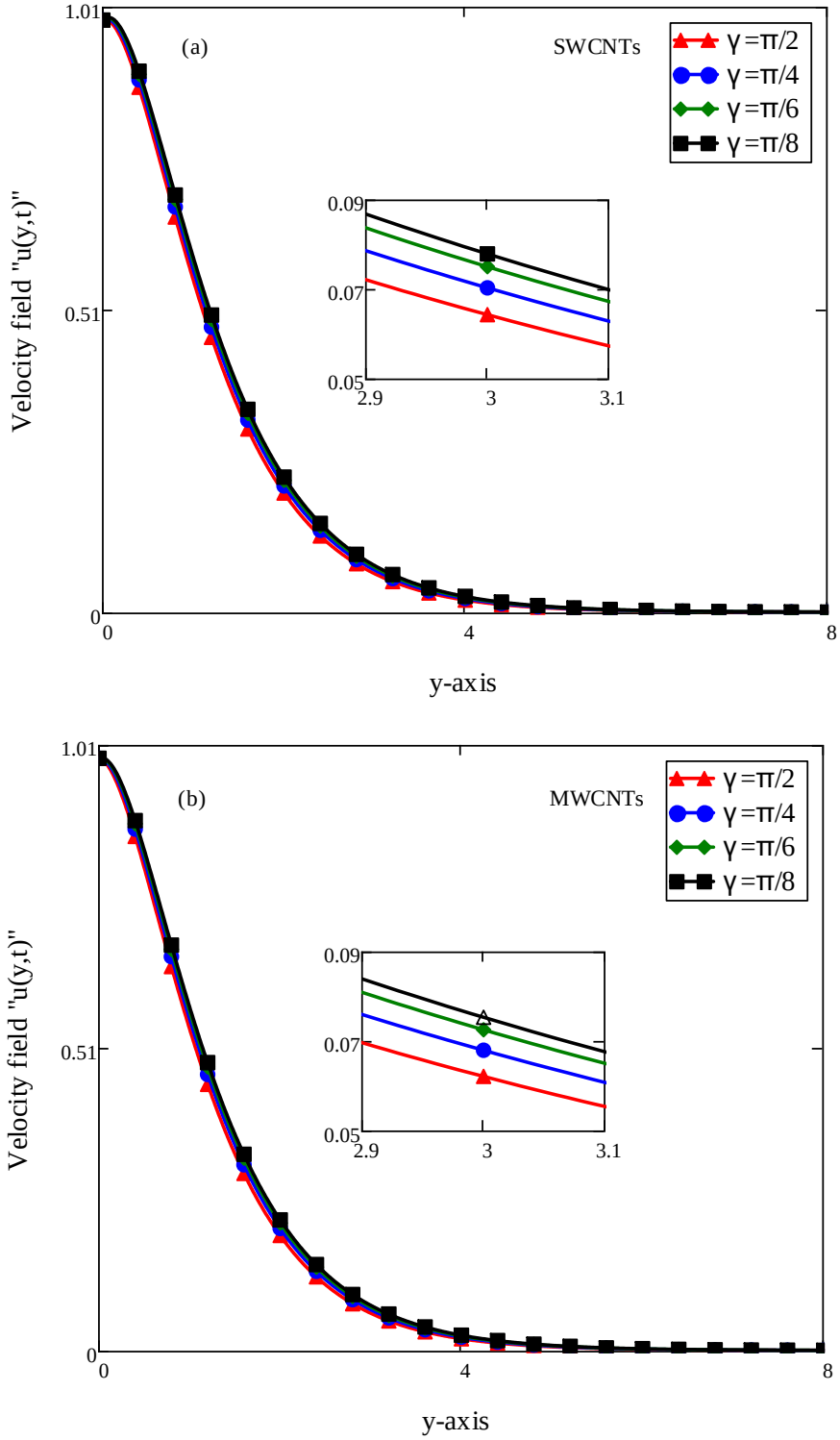

Figure 9 *Consequences of* γ *on* $u(y,t)$ *when* $t=0.5$, $\phi=0.04$ $\beta=0.5$, $M=0.5$, $K=0.5$ $Gr=7.0$, $\Pr=21$ *and* $\alpha=0.5$

Preprints (www.preprints.org) | NOT PEER-REVIEWED | Posted: 7 April 2020 doi:10.20944/preprints202004.0088.v1

Peer-reviewed version available at Symmetry 2020, 12, 768; doi:10.3390/sym12050768

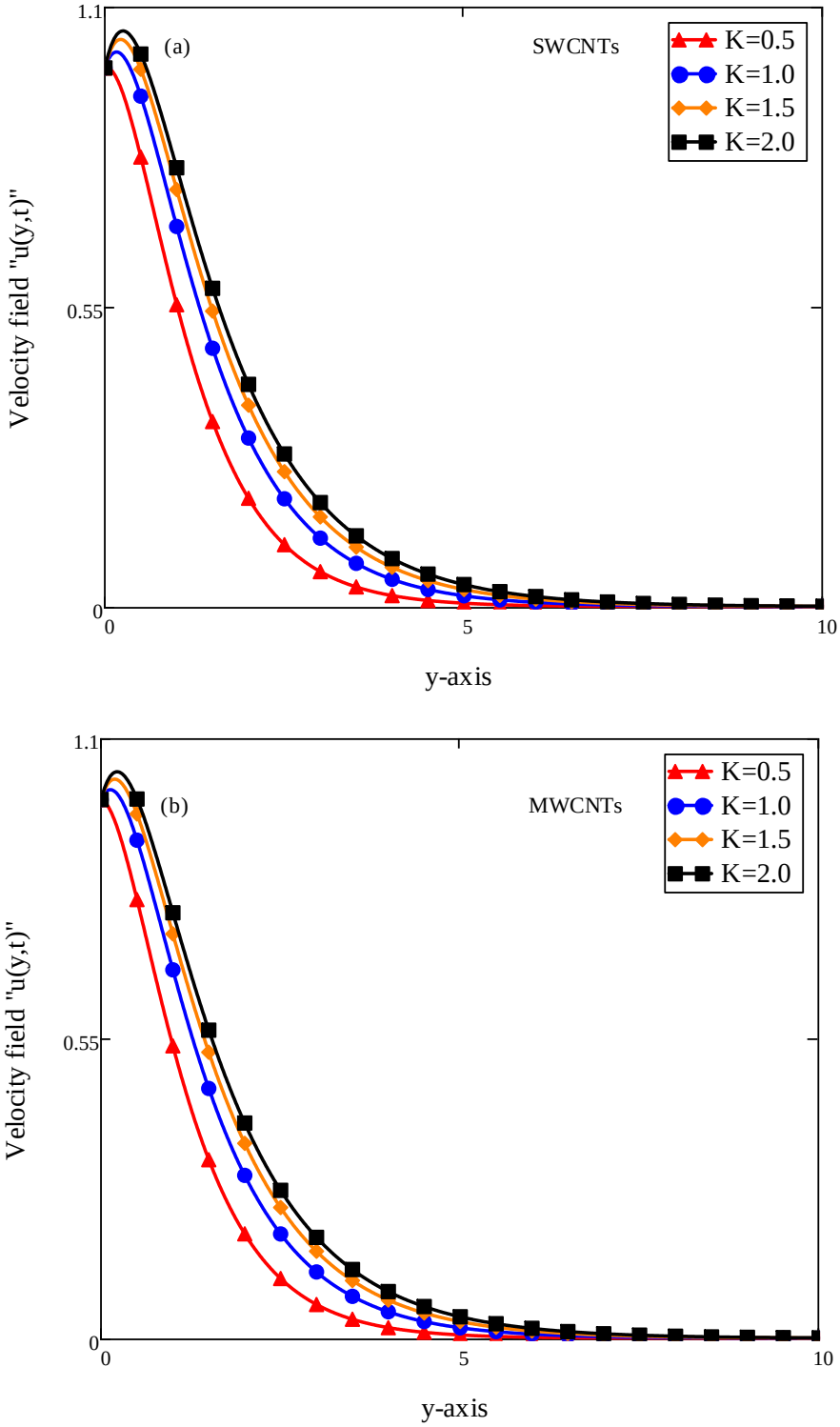

Figure 10 *Consequences of* K *on* $u(y,t)$ *when* $t=0.5$, $\phi=0.04$ $\beta=0.5$, $M=0.5$, $\gamma=\pi/2$, $Gr=7.0$, $\Pr=21$ *and* $\alpha=0.5$

Preprints (www.preprints.org) | NOT PEER-REVIEWED | Posted: 7 April 2020 doi:10.20944/preprints202004.0088.v1

Peer-reviewed version available at *Symmetry* **2020**, *12*, 768; doi:10.3390/sym12050768

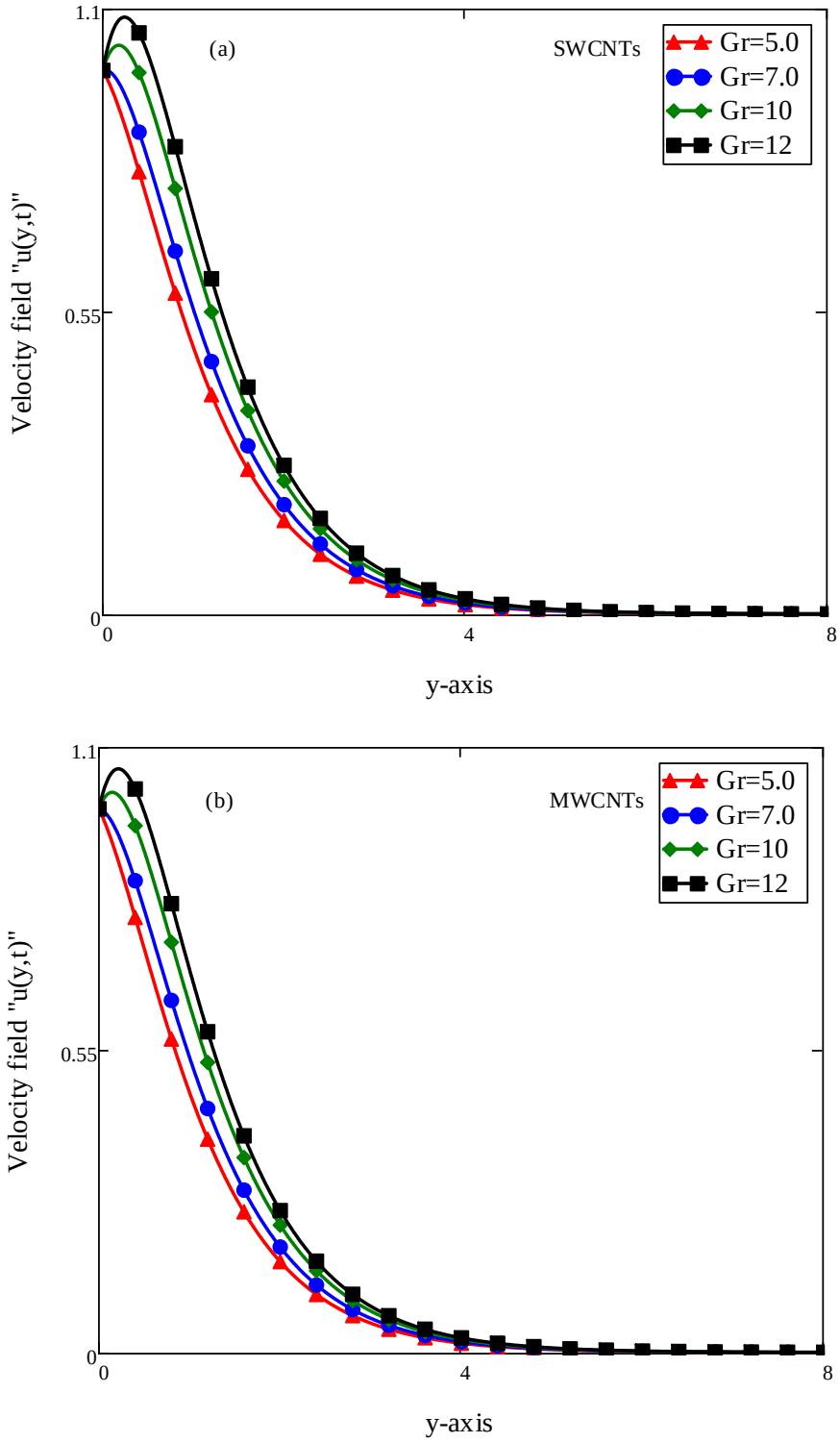

Figure 11 *Consequences of* Gr *on* $u(y,t)$ *when* $t=0.5$, $\phi=0.04$ $\beta=0.5$, $M=0.5$, $\gamma=\pi/2$, $K=0.5$, $\Pr=21$ *and* $\alpha=0.5$

REFERENCES

1. Shahsavar, A.; Sardari, P.T.; Toghraie, D. Free convection heat transfer and entropy generation analysis of water-Fe3O4/CNT hybrid nanofluid in a concentric annulus. *International Journal of Numerical Methods for Heat & Fluid Flow* **2019**.
2. Talebizadehsardari, P.; Shahsavar, A.; Toghraie, D.; Barnoon, P. An experimental investigation for study the rheological behavior of water–carbon nanotube/magnetite nanofluid subjected to a magnetic field. *Physica A: Statistical Mechanics and its Applications* **2019**, *534*, 122129.
3. Mahanthesh, B.; Lorenzini, G.; Oudina, F.M.; Animasaun, I.L. Significance of exponential space-and thermal-dependent heat source effects on nanofluid flow due to radially elongated disk with Coriolis and Lorentz forces. *Journal of Thermal Analysis and Calorimetry* **2019**, 1-8.
4. Liou, T.-M.; Wei, T.-C.; Wang, C.-S. Investigation of nanofluids on heat transfer enhancement in a louvered microchannel with lattice Boltzmann method. *Journal of Thermal Analysis and Calorimetry* **2019**, *135*, 751-762.
5. Mebarek-Oudina, F.; Bessaïh, R. Numerical simulation of natural convection heat transfer of copper-water nanofluid in a vertical cylindrical annulus with heat sources. *Thermophysics and Aeromechanics* **2019**, *26*, 325-334.
6. Raza, J.; Mebarek-Oudina, F.; Mahanthesh, B. Magnetohydrodynamic flow of nano Williamson fluid generated by stretching plate with multiple slips. *Multidiscipline Modeling in Materials and Structures* **2019**.
7. Álvarez-Regueiro, E.; Vallejo, J.P.; Fernández-Seara, J.; Fernández, J.; Lugo, L. Experimental convection heat transfer analysis of a nano-enhanced industrial coolant. *Nanomaterials* **2019**, *9*, 267.
8. O Alzahrani, E.; Shah, Z.; Alghamdi, W.; Zaka Ullah, M. Darcy–Forchheimer Radiative Flow of Micropoler CNT Nanofluid in Rotating Frame with Convective Heat Generation/Consumption. *Processes* **2019**, *7*, 666.
9. Gul, T.; Khan, M.A.; Noman, W.; Khan, I.; Abdullah Alkanhal, T.; Tlili, I. Fractional order forced convection carbon nanotube nanofluid flow passing over a thin needle. *Symmetry* **2019**, *11*, 312.

10. Hussanan, A.; Khan, I.; Gorji, M.R.; Khan, W.A. CNT S-Water–Based Nanofluid Over a Stretching Sheet. *BioNanoScience* **2019**, *9*, 21-29.
11. Jabbari, F.; Rajabpour, A.; Saedodin, S. Viscosity of carbon nanotube/water nanofluid. *Journal of Thermal Analysis and Calorimetry* **2019**, *135*, 1787-1796.
12. Kumam, P.; Shah, Z.; Dawar, A.; Rasheed, H.U.; Islam, S. Entropy generation in MHD radiative flow of CNTs Casson nanofluid in rotating channels with heat source/sink. *Mathematical Problems in Engineering* **2019**, *2019*.
13. Murshed, S.S.; De Castro, C.N. Superior thermal features of carbon nanotubes-based nanofluids–A review. *Renewable and Sustainable Energy Reviews* **2014**, *37*, 155-167.
14. Motevasel, M.; Soleimanynazar, A.; Jamialahmadi, M. Forced Convective Heat Transfer of Nano fluids: A Review of the Recent Literature. *American Journal of Oil and Chemical Technologies* **2014**, 105-118.
15. Sundar, L.S.; Sharma, K.; Naik, M.; Singh, M.K. Empirical and theoretical correlations on viscosity of nanofluids: a review. *Renewable and sustainable energy reviews* **2013**, *25*, 670-686.
16. Saqib, M.; Khan, I.; Shafie, S. Application of Atangana–Baleanu fractional derivative to MHD channel flow of CMC-based-CNT's nanofluid through a porous medium. *Chaos, Solitons & Fractals* **2018**, *116*, 79-85.
17. Murshed, S.S.; De Castro, C.N.; Lourenço, M.; Lopes, M.; Santos, F. A review of boiling and convective heat transfer with nanofluids. *Renewable and Sustainable Energy Reviews* **2011**, *15*, 2342-2354.
18. Xie, H.; Chen, L. Review on the preparation and thermal performances of carbon nanotube contained nanofluids. *Journal of Chemical & Engineering Data* **2011**, *56*, 1030-1041.
19. Sarafraz, M.; Nikkhah, V.; Nakhjavani, M.; Arya, A. Fouling formation and thermal performance of aqueous carbon nanotube nanofluid in a heat sink with rectangular parallel microchannel. *Applied Thermal Engineering* **2017**, *123*, 29-39.
20. Selimefendigil, F.; Öztop, H.F. Corrugated conductive partition effects on MHD free convection of CNT-water nanofluid in a cavity. *International Journal of Heat and Mass Transfer* **2019**, *129*, 265-277.

21. Mohd-Ghazali, N.; Estellé, P.; Halelfadl, S.; Maré, T.; Siong, T.C.; Abidin, U. Thermal and hydrodynamic performance of a microchannel heat sink with carbon nanotube nanofluids. *Journal of Thermal Analysis and Calorimetry* **2019**, *138*, 937-945.
22. Abdeen, D.H.; Atieh, M.A.; Merzougui, B.; Khalfaoui, W. Corrosion Evaluation of 316L Stainless Steel in CNT-Water Nanofluid: Effect of CNTs Loading. *Materials* **2019**, *12*, 1634.
23. Abro, K.A.; Atangana, A. A comparative study of convective fluid motion in rotating cavity via Atangana–Baleanu and Caputo–Fabrizio fractal–fractional differentiations. *The European Physical Journal Plus* **2020**, *135*, 226.
24. Atangana, A.; Aguilar, J.F.G.; Kolade, M.O.; Hristov, J.Y. Fractional differential and integral operators with non-singular and non-local kernel with application to nonlinear dynamical systems. *CSF* **2020**, *132*, 109493.
25. Dubey, V.P.; Kumar, R.; Kumar, D.; Khan, I.; Singh, J. An efficient computational scheme for nonlinear time fractional systems of partial differential equations arising in physical sciences. *Advances in Difference Equations* **2020**, *2020*, 46.
26. Heydari, M.; Atangana, A. An optimization method based on the generalized Lucas polynomials for variable-order space-time fractional mobile-immobile advection-dispersion equation involving derivatives with non-singular kernels. *Chaos, Solitons & Fractals* **2020**, *132*, 109588.
27. Suthar, D.; Khan, A.; Alaria, A.; Purohit, S.; Singh, J. Extended Bessel-Maitland function and its properties pertaining to integral transforms and fractional calculus. *AIMS Mathematics* **2020**, *5*, 1400.
28. Veeresha, P.; Prakasha, D.; Singh, J. Solution for fractional forced KdV equation using fractional natural decomposition method. **2019**.
29. Veeresha, P.; Prakasha, D.; Singh, J. A novel approach for nonlinear equations occurs in ion acoustic waves in plasma with Mittag-Leffler law. *Engineering Computations* **2020**.
30. Podlubny, I. *Fractional differential equations: an introduction to fractional derivatives, fractional differential equations, to methods of their solution and some of their applications*; Elsevier: 1998.
31. Caputo, M. Linear models of dissipation whose Q is almost frequency independent. *Annals of Geophysics* **1966**, *19*, 383-393.

32. Caputo, M. Linear models of dissipation whose Q is almost frequency independent—II. *Geophysical Journal International* **1967**, *13*, 529-539.
33. Caputo, M.; Fabrizio, M. A new definition of fractional derivative without singular kernel. *Progr. Fract. Differ. Appl* **2015**, *1*, 1-13.
34. Atangana, A.; Doungmo Goufo, E. A model of the groundwater flowing within a leaky aquifer using the concept of local variable order derivative. *Journal of Nonlinear Science and Applications* **2015**, *8*, 763-775.
35. Ali, F.; Sheikh, N.A.; Khan, I.; Saqib, M. Solutions with Wright function for time fractional free convection flow of Casson fluid. *Arabian Journal for Science and Engineering* **2017**, *42*, 2565-2572.
36. Khalid, A.; Khan, I.; Khan, A.; Shafie, S.; Tlili, I. Case study of MHD blood flow in a porous medium with CNTS and thermal analysis. *Case studies in thermal engineering* **2018**, *12*, 374-380.
37. Saqib, M.; Khan, I.; Shafie, S. Generalized magnetic blood flow in a cylindrical tube with magnetite dusty particles. *Journal of Magnetism and Magnetic Materials* **2019**, *484*, 490-496.
38. Ali, F.; Saqib, M.; Khan, I.; Sheikh, N.A.; Jan, S.A.A. Exact analysis of MHD flow of a Walters'-B fluid over an isothermal oscillating plate embedded in a porous medium. *The European Physical Journal Plus* **2017**, *132*, 95.
39. Sheikh, N.A.; Ching, D.L.C.; Khan, I.; Kumar, D.; Nisar, K.S. A new model of fractional Casson fluid based on generalized Fick's and Fourier's laws together with heat and mass transfer. *Alexandria Engineering Journal* **2019**.
40. Ali, F.; Saqib, M.; Khan, I.; Sheikh, N.A. Application of Caputo-Fabrizio derivatives to MHD free convection flow of generalized Walters'-B fluid model. *The European Physical Journal Plus* **2016**, *131*, 377.
41. Saqib, M.; Khan, I.; Shafie, S.; Qushairi, A. Recent Advancement inThermophysical Properties of Nanofluids and Hybrid nanofluids: An Overvies. *City University International Journal of Computational Analysis* **2020**, *1(2)*, 16-25.
42. Jan, S.A.A.; Ali, F.; Sheikh, N.A.; Khan, I.; Saqib, M.; Gohar, M. Engine oil based generalized brinkman-type nano-liquid with molybdenum disulphide nanoparticles of

spherical shape: Atangana-Baleanu fractional model. *Numerical Methods for Partial Differential Equations* **2018**, *34*, 1472-1488.

43. Shafie, S.; Saqib, M.; Khan, I.; Qushairi, A. Mixed Convection Flow of Brinkman Type Hybrid Nanofluid Based on Atangana-Baleanu Fractional Model. In Proceedings of Journal of Physics: Conference Series; p. 012041.
44. Saqib, M.; Khan, I.; Shafie, S. Shape Effect in Magnetohydrodynamic Free Convection Flow of Sodium Alginate-Ferrimagnetic Nanofluid. *Journal of Thermal Science and Engineering Applications* **2019**, *11*.
45. Ali, F.; Sheikh, N.A.; Khan, I.; Saqib, M. Magnetic field effect on blood flow of Casson fluid in axisymmetric cylindrical tube: A fractional model. *Journal of Magnetism and Magnetic Materials* **2017**, *423*, 327-336.
46. Khan, I.; Saqib, M.; Alqahtani, A.M. Channel flow of fractionalized H2O-based CNTs nanofluids with Newtonian heating. *Discrete & Continuous Dynamical Systems-S* **2019**, 769.